Frequency-Domain Quantum Interference with Correlated Photons from an Integrated Microresonator

Chaitali Joshi,[1,2] Alessandro Farsi,[1] Avik Dutt,[3] Bok Young Kim,[1] Xingchen Ji,[4] Yun Zhao,[4] Andrew M. Bishop,[1] Michal Lipson,[1,4] and Alexander L. Gaeta[1,4,*]

[1]*Applied Physics and Applied Mathematics, Columbia University, New York, New York 10027, USA*
[2]*Applied and Engineering Physics, Cornell University, Ithaca, New York 14850, USA*
[3]*Ginzton Laboratory and Department of Electrical Engineering, Stanford University, Stanford, California 94305, USA*
[4]*Department of Electrical Engineering, Columbia University, New York, New York 10027, USA*

(Received 3 December 2019; accepted 11 March 2020; published 6 April 2020)

Frequency encoding of quantum information together with fiber and integrated photonic technologies can significantly reduce the complexity and resource requirements for realizing all-photonic quantum networks. The key challenge for such frequency domain processing of single photons is to realize coherent and selective interactions between quantum optical fields of different frequencies over a range of bandwidths. Here, we report frequency-domain Hong-Ou-Mandel interference with spectrally distinct photons generated from a chip-based microresonator. We use four-wave mixing to implement an active "frequency beam splitter" and achieve interference visibilities of 0.95 ± 0.02. Our work establishes four-wave mixing as a tool for selective high-fidelity two-photon operations in the frequency domain which, combined with integrated single-photon sources, provides a building block for frequency-multiplexed photonic quantum networks.

DOI: 10.1103/PhysRevLett.124.143601

Two-photon interference is a fundamental quantum effect with no classical analogue. Such interference is at the heart of photonic quantum information processing (QIP) and is the basis of several QIP realizations such as Bell-state measurement, boson sampling, measurement-based logic gates, and the generation of multipartite entangled Greenberger-Horne-Zeilinger (GHZ) and cluster states [1–4]. In the original Hong-Ou-Mandel (HOM) interference experiment, the photon wave packets are in distinct spatial modes [5], but are otherwise identical in their polarization, spectral, and temporal properties at the input. However, subsequent experimental and theoretical work confirms it is the indistinguishability of the two-photon amplitudes at the output of the interferometer that is crucial to the observation of HOM-type interference [6]. This leads to the interesting possibility of observing quantum interference involving spectrally distinct photons. An "active" device that coherently mixes two input frequency modes can render distinct spectral amplitudes indistinguishable, resulting in fourth-order interference with the two photons bunched in the same frequency mode [7].

In this Letter, we combine frequency-entangled photons generated on chip together with Bragg-scattering four-wave mixing (BS-FWM) in optical fiber to demonstrate frequency-domain HOM interference visibilities as high as 95%. We show interference with narrow photons less than 300 MHz in bandwidth and widely separated in frequency by 800 GHz. We predict and observe a rich two-photon interference pattern, including the phenomenon of quantum beating in the temporal domain. Novel approaches for all-photonic quantum repeaters rely on a combination of efficient single-photon sources, linear operations with beam splitters and measurement-based fusion gates to generate entangled multiphoton GHZ and cluster states [8,9]. Frequency multiplexing can massively reduce the resource requirements for such all-photonic quantum networks. Frequency domain quantum operations also provide a distinct advantage in terms of the scaling of losses over spatial or polarization mode processing [10–12]. Cavity-enhanced spontaneous four-wave mixing (SFWM) in integrated microresonators produces frequency-entangled photon pairs with an effectively discrete joint spectral intensity [13–17]. A large number of such compact, identical sources can be integrated on a monolithic platform for the generation and manipulation of complex nonclassical states of light [18–21]. Our demonstration establishes BS-FWM as a tool for selective, high-fidelity two-photon operations between frequency modes of integrated microresonators.

BS-FWM is a unitary, third-order parametric process in which two strong classical pump waves mediate the interaction between the quantum fields via a third order ($\chi^{(3)}$) nonlinearity [Figs. 1(a) and 1(b)] [22–26]. By controlling the power and phase of the classical fields involved, we emulate a tunable active frequency beam splitter [27]. For quantum frequency conversion based on $\chi^{(2)}$ nonlinearity, the input and target modes must be placed in different optical bands,

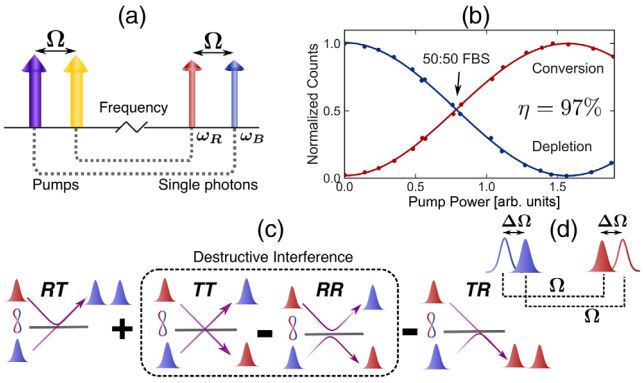

FIG. 1. Frequency beam splitter via BS-FWM: (a) Two strong classical pumps $(\omega_{P1}, \omega_{P2})$ mediate the interaction between two quantum fields, (ω_R, ω_B) in a medium with third-order $\chi^{(3)}$ nonlinearity. (b) Measured signal conversion and depletion (efficiency $\eta = 97\%$). BS-FWM acts as a 50:50 frequency beam splitter (FBS) when the pump power is such that the nonlinear interaction strength $\gamma PL = \pi/8$. (c) Two frequency-correlated photons incident on a 50:50 FBS. Perfect HOM-type interference is observed when the two-photon amplitude for both photons being frequency translated (RR) and neither photon being translated (TT) are indistinguishable. This occurs when the BS-FWM pump separation Ω matches the input photon-pair separation, resulting in $\Delta\Omega = 0$ [see (d)].

typically separated by few tens to a hundred THz in order to satisfy energy conservation. Alternatively, electro-optic modulators (EOMs) can impart only small frequency shifts of the order of a few gigahertz. With BS-FWM, the use of two classical fields provides an additional degree of freedom, and efficient conversion is possible for separations ranging from a few hundred GHz to a few THz [11]. This makes a BS-FWM frequency beam splitter (FBS) compatible with the typical free spectral range (FSR) of integrated microresonators and, also, with dense wavelength division multiplexing (WDM) components aligned to the international telecommunication union (ITU) grid. Previously, EOMs have been used in combination with integrated sources to generate high-dimensional time-frequency entangled states [28–30]. Together with pulse shaping and bulk single-photon sources, EOMs have also been used to create frequency-bin entangled states and to demonstrate two-photon HOM-type interference with modes separated by up to 25 GHz [31–37]. Recently, frequency translation in a $\chi^{(2)}$ crystal was used to demonstrate interference between a single photon and attenuated coherent laser light [38].

We use quantum frequency translation via BS-FWM to create a coherent interaction between two quantum fields at different frequencies (ω_R, ω_B), as shown in Fig. 1. Energy conservation requires that the frequency separation between the classical pump fields $(\omega_{P1} - \omega_{P2} = \Omega)$ should match the separation of the quantum fields $(\omega_B - \omega_R = \Omega)$. Phase matching $(\Delta\beta = \beta_R + \beta_{P1} - \beta_B - \beta_{P2}$, β: propagation constant) can be ensured by placing the pump fields and the quantum fields symmetrically about the zero group-velocity dispersion, $\beta^{(2)} = 0$) point of the interaction medium. Because of the effects of third-order dispersion $(\beta^{(3)})$, it is possible to ensure selective phase matching such that the resulting process is a two-mode interaction without spurious side-bands (see Supplemental Material [39] Sec. S1). For such a selectively phase-matched process $(\Delta\beta = 0)$, the mode transformations for signal and idler annihilation operators $\hat{a}(\omega_R), \hat{a}(\omega_B)$ after passing through the FBS are given by

$$\begin{aligned} \hat{a}_R(\omega_R) &\to \upsilon \hat{a}_R(\omega_R) - \mu \hat{a}_B(\omega_R + \Omega), \\ \hat{a}_B(\omega_B) &\to \mu^* \hat{a}_R(\omega_B - \Omega) + \upsilon^* \hat{a}_B(\omega_B), \end{aligned} \tag{1}$$

where $\upsilon = \cos(2\gamma PL), \mu = e^{i\phi}\sin(2\gamma PL)$, Ω is the frequency separation of the two pump fields, $P = \sqrt{P_1 P_2}$ depends on the power P_1, P_2 of the two classical pumps, γ is proportional to the nonlinearity of the interaction medium, L is the interaction length, ϕ is the relative phase between the pumps. The subscripts (R, B) denote the red-detuned and blue-detuned frequencies, respectively. As is evident from Eq. (1) and as demonstrated in Ref. [27], BS-FWM acts as an $SU(2)$ transformation and can produce arbitrary single-qubit rotations in the two-dimensional frequency Hilbert space $\{|\omega_R\rangle, |\omega_B\rangle\}$.

Here, we formally establish that this process can be used for two-photon quantum interference [see Figs. 1(b) and 1(c) and Supplemental Material [39] Sec. 2]. We theoretically predict the conditions for observing perfect Hong-Ou-Mandel type interference for two frequency-correlated photons and show that our experimental findings are in excellent agreement with these theoretical predictions. The initial two-photon wave-function is given as

$$|\psi\rangle = \int d\omega_B d\omega_R \phi(\omega_B, \omega_R) \hat{a}_R^\dagger(\omega_R) \hat{a}_B^\dagger(\omega_B) |0, 0\rangle, \tag{2}$$

where $\phi(\omega_R, \omega_B)$ is the joint spectral amplitude (JSA) of the two photons. The coincidence measurement at the output corresponds to the two-photon correlation function

$$G^{(2)}(\tau) = \langle E_R^{(-)}(t) E_B^{(-)}(t+\tau) E_B^{(+)}(t+\tau) E_R^{(+)}(t) \rangle. \tag{3}$$

The quantized electric field is related to the annihilation operator as $E^{(+)}(t) = [E^{(-)}(t)]^\dagger \propto 1/\sqrt{(2\pi)} \int d\omega \hat{a}(\omega) e^{-i\omega t}$. Combining Eqs. (2) and (3) and using standard commutation relations, we obtain

$$\begin{aligned} G^{(2)}(\tau) = \int & d\omega'_R d\omega'_B d\omega_R d\omega_B e^{i(\omega'_R - \omega_R)(\tau)} \\ & \times \phi^*(\omega'_B, \omega'_R) \phi(\omega_B, \omega_R). \end{aligned} \tag{4}$$

As expected, the second-order correlation function is the Fourier transform of the joint spectral intensity of the photons. We calculate the second-order correlation function after the photons have undergone the transformation in

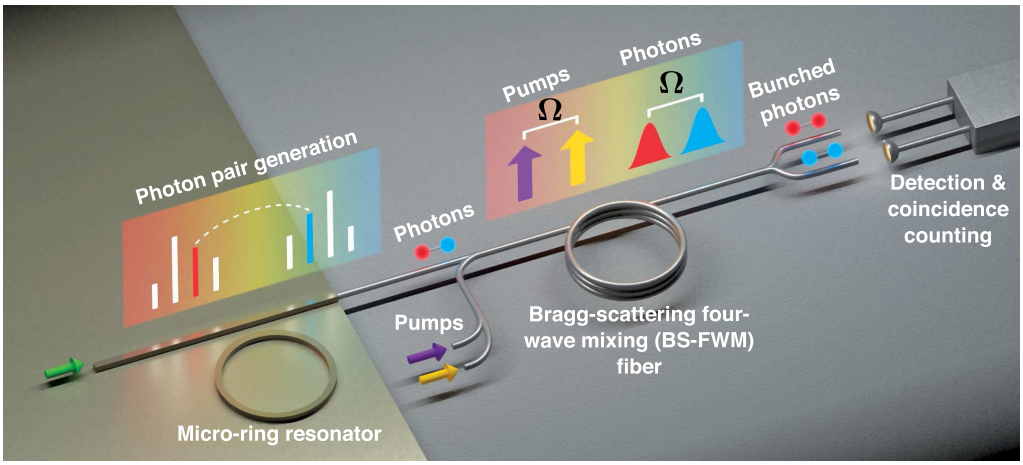

FIG. 2. Frequency domain two-photon interference via BS-FWM: Narrow band frequency-correlated photons are generated via spontaneous four-wave mixing (SFWM) in a silicon nitride microring resonator. The generated photons are coupled together with two classical pump waves through a WDM into a dispersion-shifted fiber for Bragg-scattering four-wave mixing (BS-FWM). The power of the BS-FWM pumps is set such that it acts as a 50:50 frequency beam splitter and their frequency separation Ω is set to precisely match the selected pair of correlated photons. After the nonlinear interaction, the two frequency arms are separated through a WDM followed by detection and coincidence counting. Hong-Ou-Mandel type interference is observed and both photons are bunched in the same frequency mode.

Eq. (1). Combining Eqs. (1), (2), and (3) for the case $\upsilon = \mu = 1/\sqrt{2}$, we obtain

$$\begin{aligned} G^{(2)}(\tau) = \frac{1}{4}\int & d\omega'_R d\omega'_B d\omega_R d\omega_B e^{i(\omega'_R-\omega_R)(\tau)} \\ & \times [\phi^*(\omega'_B,\omega'_R)\phi(\omega_B,\omega_R) \\ & - \phi^*(\omega'_B,\omega'_R)\phi(\omega_R+\Omega,\omega_B-\Omega) \\ & + \phi^*(\omega'_R+\Omega,\omega'_B-\Omega)\phi(\omega_R+\Omega,\omega_B-\Omega) \\ & - \phi^*(\omega'_R+\Omega,\omega'_B-\Omega)\phi(\omega_B,\omega_R)], \end{aligned} \tag{5}$$

where we assume that the integration limits are well within the phase-matching bandwidth of BS-FWM. From Eq. (5), it is seen that perfect destructive interference occurs when the two-photon amplitude associated with both photons being frequency translated is indistinguishable from the two-photon amplitude for the case in which neither photon undergoes translation, that is, when $\phi(\omega_B,\omega_R) = \phi(\omega_R+\Omega,\omega_B-\Omega)$.

Equations (4) and (5) can be explicitly evaluated for the case of photon pairs generated via cw-pumped SFWM in a ring resonator. The JSA for photon pairs generated in two symmetrically placed resonances (ω_R^0,ω_B^0) about the resonance corresponding to the SFWM pump is, $\phi(\omega_B,\omega_R) \propto \delta(\omega_R+\omega_B-2\omega_P) l(\omega_B,\omega_B^0) l(\omega_R,\omega_R^0)$ where ω_P is the SFWM pump frequency, $l(\omega,\omega^0) = (\Delta\omega/2)^{\frac{1}{2}}/[-i(\omega-\omega^0)+(\Delta\omega/2)]$, such that $|l(\omega,\omega^0)|^2$ describes the Lorentzian response of a ring resonance centered at ω^0 with a full-width at half maximum $\Delta\omega$ [40]. Equation (4) then reduces to

$$G^{(2)}(\tau) \propto e^{-\Delta\omega|\tau|}. \tag{6}$$

Similarly, evaluating Eq. (5) results in the second-order coherence function after the 50:50 FBS

$$G^{(2)}(\tau) \propto e^{-\Delta\omega|\tau|}\sin^2\left(\frac{\Delta\Omega\tau}{2}\right), \tag{7}$$

where we have introduced the variable $\Delta\Omega = \Omega - (\omega_B^0 - \omega_R^0)$ to reflect the offset between the frequency separation Ω of the BS-FWM pumps with respect to the separation of the photon envelopes centered at ω_B^0 and ω_R^0. Equation (7) shows that the observed interference depends sensitively on the offset $\Delta\Omega$. When $\Delta\Omega = 0$, $G^{(2)}(\tau) = 0$ for all τ, as expected from the fact that two-photon wave functions before and after frequency translation are completely indistinguishable. For offsets $\Delta\Omega$ that are small or comparable to the resonator linewidth $\Delta\omega$, the phenomenon of quantum beating is predicted [41]. We note that this beating can only be resolved if $2\pi/\Delta\Omega$ is much larger than the temporal resolution of the single-photon detectors [42].

We experimentally demonstrate this detuning-dependent HOM interference in agreement with these theoretical predictions using the scheme depicted in Fig. 2. A silicon nitride microresonator is pumped with a cw laser at 1282.8 nm to generate frequency-correlated photon pairs in the O band through SFWM. The generated photons are coupled into a single-mode fiber and combined with the classical pump fields located in the C band for BS-FWM and sent to a dispersion-shifted fiber (Corning Vistacor). The BS-FWM pumps are intensity modulated to generate 10-ns long pulses that are amplified with an erbium-doped

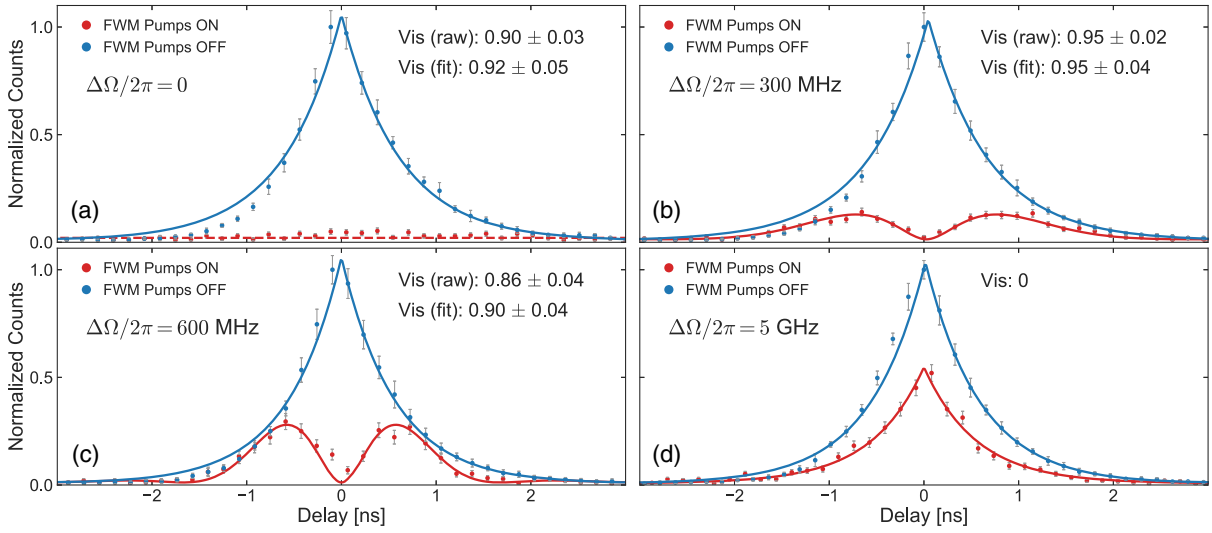

FIG. 3. Experimental observation of frequency domain two-photon interference. Red curves and blue curves (dots: experiment, solid line: fit) are the normalized threefold coincidence counts when the BS-FWM pumps are on and off, respectively. The photon bandwidth is measured to be 270 ± 15 MHz. (a) When $\Delta\Omega = 0$, we observe a flat $G^{(2)}(\tau)$ with a raw visibility $\alpha_r = 0.90 \pm 0.03$ (fit visibility $\alpha_f = 0.92 \pm 0.05$. (b) For a detuning $\Delta\Omega/2\pi = 300$ MHz, we observe temporal beating with a raw visibility $\alpha_r = 0.95 \pm 0.02$ (fit visibility $\alpha_f = 0.95 \pm 0.04$). (c) For $\Delta\Omega/2\pi = 600$ MHz, we observe an increase in the amplitude of the side lobes of the beating signal with a measured raw visibility of $\alpha_r = 0.86 \pm 0.04$ (fit visibility $\alpha_f = 0.90 \pm 0.04$). (d) For very large detuning ($\Delta\Omega/2\pi = 5$ GHz), the interference fringes are no longer resolved resulting in a double-exponential output ($\alpha = 0$). Error bars are calculated assuming Poisson statistics.

fiber amplifier. The polarizations of the BS-FWM pumps are aligned to the linear polarization of the input state to achieve more than 95% depletion. The pump power is then set to obtain 50% depletion such that the photons now see a device that emulates a 50:50 FBS. The two frequency arms are separated using a WDM followed by free space grating filters to extract photons that are red detuned (centered at ω_R^0) and blue detuned (centered at ω_B^0) by two FSRs with respect to the SFWM pump. The photons are then detected with superconducting nanowire single photon detectors, followed by coincidence counting using a time-tagging module. In order to match the BS-FWM pump separation Ω precisely to that of the two photons ($\omega_B^0 - \omega_R^0$), we perform a precise measurement of the FSR with a phase modulator (see Supplemental Material [39] Sec. III). We measure an FSR of 201.275 GHz, resulting in a photon separation $(\omega_B^0 - \omega_R^0)/2\pi = 805.1$ GHz. A detailed description of the experimental system, including characterization of losses is included in Supplemental Material [39] Sec. III.

Our experimental results are shown in Fig. 3 and are in excellent agreement with our theoretical predictions. We obtain a photon bandwidth $\Delta\omega/2\pi = 270 \pm 15$ MHz from the measured cross correlation $G^{(2)}(\tau)$. In order to post-select only those photon coincidences that occur within the 10-ns temporal window of the BS-FWM pumps, we perform a threefold coincidence measurement with the arrival time of the two photons at the superconducting nanowire single-photon detectors (SNSPDs) and a synchronization signal from the pumps. We then obtain suitable normalization by averaging over coincidences accumulated in 10-ns temporal windows that are not synchronized with the BS-FWM pumps (Fig. 3, blue curves, see, also, Supplemental Material [39] Sec. III). For an integration time of one hour, we measure 2700 threefold normalization coincidence counts within the $1/e$ coherence time of the photons. We introduce a visibility parameter α in Eq. (7), such that $G^{(2)}(\tau) \propto e^{-\Delta\omega|\tau|}((1/2) - (\alpha/2)\cos\Delta\Omega\tau)$. This visibility parameter α corresponds the depth of the beating signal at $\tau = 0$ and is a direct indicator of the fidelity of our 50:50 FBS and the indistinguishability of the two-photon amplitude before and after frequency translation. Any distinguishability in other degrees of freedom such as polarization or deviation from the balanced splitting ratio degrades this extinction. As expected, when the offset $\Delta\Omega$ is zero, we observe nearly complete destructive interference resulting in a flat $G^{(2)}(\tau)$.

TABLE I. Measured two-photon interference visibilities: The measured raw visibilities (α_r) are consistent with the visibilities extracted from fit to the data (α_f) within our measurement error, indicating excellent agreement between our theory and experiment.

Detuning $\Delta\Omega$ (MHz)	Raw visibility (α_r)	Fit visibility (α_f)
0	0.90 ± 0.03	0.92 ± 0.05
300	0.95 ± 0.02	0.95 ± 0.04
600	0.86 ± 0.04	0.90 ± 0.04

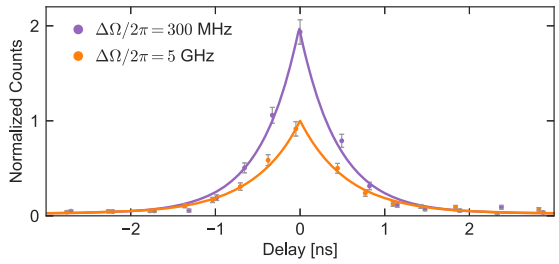

FIG. 4. Photon bunching via autocorrelation. Measured enhancement in two-photon bunching for small (purple, $\Delta\Omega/2\pi =$ 300 MHz) over large pump detunings (orange, $\Delta\Omega/2\pi = 5$ GHz) with a measured peak autocorrelation of 1.93 ± 0.13.

We measure a raw visibility of $\alpha_r = 0.90 \pm 0.03$ from the data and extract a visibility $\alpha_f = 0.92 \pm 0.05$ from fit to the data [Fig. 3(a), red curve]. For $\Delta\Omega/2\pi = 300$ MHz, we obtain a raw visibility of $\alpha_r = 0.95 \pm 0.02$ [fit visibility $\alpha_f = 0.95 \pm 0.04$, Fig. 3(b)]. The high visibility of these measurements indicates that BS-FWM preserves the polarization and spatiotemporal modes of the input quantum fields after frequency translation. For higher detunings $\Delta\Omega = 600$ MHz, we see the expected increase in the amplitude of the side lobes [Fig. 3(c)]. We measure an interference visibility of $\alpha_r = 0.86 \pm 0.04$ (fit visibility $\alpha_f = 0.90 \pm 0.04$) from this detuning. The reduced raw visibilities in these measurements are due to fluctuations in polarization and pump power during the hour-long measurement and due to multiphoton noise (see Supplemental Material [39] Sec. III) [43,44]. For large detuning, $\Delta\Omega/2\pi = 5$ GHz, the interference fringes are no longer resolved by the detection system, resulting in a double-exponential output ($\alpha = 0$) as shown in Fig. 3(d). Our results are summarized in Table I. The measured raw visibilities are consistent with the visibilities extracted from fit to the data within our measurement error, indicating excellent agreement between our theoretical predictions and experiment.

The 50:50 FBS stochastically bunches photons to the same frequency mode with a probability 1/4 even in the absence of two-photon interference [Fig. 3(d), red curve]. This probability is enhanced by a factor of 2 in the presence of two-photon interference, resulting in near-perfect coalescence. We experimentally confirm this enhancement in bunching with a second-order auto correlation measurement on the blue-detuned (ω_B) frequency arm. As shown in Fig. 4, we observe an enhancement for small pump detunings $\Delta\Omega/2\pi = 300$ MHz as compared to the case with large pump detunings $\Delta\Omega/2\pi = 5$ GHz, with a measured peak autocorrelation of 1.93 ± 0.13.

In conclusion, we have demonstrated two-photon interference in the frequency domain using an on-chip photon source with visibilities as high as 95%. In contrast to experiments based on bulk photon sources and free-space optics, we observe interference in a single spatial mode, and do not require active stabilization or alignment of interferometric paths to achieve high visibility. Selective two-photon operations are possible between arbitrary pairs of resonator modes over a large bandwidth up to a few THz [see Supplemental Material [39] Fig. 1(d)] [11]. While multiplexing several two-photon operations will be associated with a classical resource overhead for the preparation of additional BS-FWM pumps, no additional components or losses are introduced in the paths of the photons (see Supplemental Material [39] Sec. IV). Our demonstration can be extended to spectrally pure single photons generated via pulsed excitation of the microresonator [40,45]. Together with implementations of BS-FWM in nanophotonic devices [46–49], such two photon operations can be used for the on chip generation of multipartite entangled GHZ and cluster states. Our demonstration offers a path to combining on-chip photon sources, fiber-based wavelength division multiplexing, and four-wave mixing for the realization of scalable frequency-multiplexed photonic quantum repeaters and networks.

We acknowledge useful discussions with Aseema Mohanty, Yoshitomo Okawachi, Rajveer Nehra, Ben Sparkes, and Jakob Gillespie. This work was funded by the National Science Foundation under Grants No. PHY-1707918 and No. OMA-1936345.

*a.gaeta@columbia.edu

[1] D. Bouwmeester, J.-W. Pan, M. Daniell, H. Weinfurter, and A. Zeilinger, Observation of Three-Photon Greenberger-Horne-Zeilinger Entanglement, Phys. Rev. Lett. **82**, 1345 (1999).
[2] E. Knill, R. Laflamme, and G. J. Milburn, A scheme for efficient quantum computation with linear optics, Nature (London) **409**, 46 (2001).
[3] J. B. Spring, B. J. Metcalf, P. C. Humphreys, W. S. Kolthammer, X.-M. Jin, M. Barbieri, A. Datta, N. Thomas-Peter, N. K. Langford, D. Kundys, J. C. Gates, B. J. Smith, P. G. R. Smith, and I. A. Walmsley, Boson sampling on a photonic chip, Science **339**, 798 (2013).
[4] F. Ewert and P. van Loock, 3/4-Efficient Bell Measurement with Passive Linear Optics and Unentangled Ancillae, Phys. Rev. Lett. **113**, 140403 (2014).
[5] C. K. Hong, Z. Y. Ou, and L. Mandel, Measurement of Subpicosecond Time Intervals Between Two Photons by Interference, Phys. Rev. Lett. **59**, 2044 (1987).
[6] T. B. Pittman, D. V. Strekalov, A. Migdall, M. H. Rubin, A. V. Sergienko, and Y. H. Shih, Can Two-Photon Interference be Considered the Interference of Two Photons?, Phys. Rev. Lett. **77**, 1917 (1996).
[7] M. G. Raymer, S. J. van Enk, C. J. McKinstrie, and H. J. McGuinness, Interference of two photons of different color, Opt. Commun. **283**, 747 (2010).
[8] M. Zwerger, W. Dür, and H. J. Briegel, Measurement-based quantum repeaters, Phys. Rev. A **85**, 062326 (2012).
[9] K. Azuma, K. Tamaki, and H.-K. Lo, All-photonic quantum repeaters, Nat. Commun. **6**, 6787 (2015).

[10] J. M. Lukens and P. Lougovski, Frequency-encoded photonic qubits for scalable quantum information processing, Optica **4**, 8 (2017).
[11] C. Joshi, A. Farsi, S. Clemmen, S. Ramelow, and A. L. Gaeta, Frequency multiplexing for quasi-deterministic heralded single-photon sources, Nat. Commun. **9**, 847 (2018).
[12] T. Hiemstra, T. F. Parker, P. C. Humphreys, J. Tiedau, M. Beck, M. Karpiński, B. J. Smith, A. Eckstein, W. S. Kolthammer, and I. A. Walmsley, Pure single photons from scalable frequency multiplexing, arXiv:1907.10355.
[13] C. Reimer, L. Caspani, M. Clerici, M. Ferrera, M. Kues, M. Peccianti, A. Pasquazi, L. Razzari, B. E. Little, S. T. Chu, D. J. Moss, and R. Morandotti, Integrated frequency comb source of heralded single photons, Opt. Express **22**, 6535 (2014).
[14] N. C. Harris, D. Grassani, A. Simbula, M. Pant, M. Galli, T. Baehr-Jones, M. Hochberg, D. Englund, D. Bajoni, and C. Galland, Integrated Source of Spectrally Filtered Correlated Photons for Large-Scale Quantum Photonic Systems, Phys. Rev. X **4**, 041047 (2014).
[15] S. Ramelow, A. Farsi, S. Clemmen, D. Orquiza, K. Luke, M. Lipson, and A. L. Gaeta, Silicon-nitride platform for narrowband entangled photon generation, arXiv:1508.04358.
[16] W. C. Jiang, X. Lu, J. Zhang, O. Painter, and Q. Lin, Silicon-chip source of bright photon pairs, Opt. Express **23**, 20884 (2015).
[17] D. Grassani, S. Azzini, M. Liscidini, M. Galli, M. J. Strain, M. Sorel, J. E. Sipe, and D. Bajoni, Micrometer-scale integrated silicon source of time-energy entangled photons, Optica **2**, 88 (2015).
[18] N. Montaut, L. Sansoni, E. Meyer-Scott, R. Ricken, V. Quiring, H. Herrmann, and C. Silberhorn, High-Efficiency Plug-and-Play Source of Heralded Single Photons, Phys. Rev. Applied **8**, 024021 (2017).
[19] E. Meyer-Scott, N. Prasannan, C. Eigner, V. Quiring, J. M. Donohue, S. Barkhofen, and C. Silberhorn, High-performance source of spectrally pure, polarization entangled photon pairs based on hybrid integrated-bulk optics, Opt. Express **26**, 32475 (2018).
[20] X. Qiang, X. Zhou, J. Wang, C. M. Wilkes, T. Loke, S. O'Gara, L. Kling, G. D. Marshall, R. Santagati, T. C. Ralph, J. B. Wang, J. L. O'Brien, M. G. Thompson, and J. C. F. Matthews, Large-scale silicon quantum photonics implementing arbitrary two-qubit processing, Nat. Photonics **12**, 534 (2018).
[21] S. Paesani, Y. Ding, R. Santagati, L. Chakhmakhchyan, C. Vigliar, K. Rottwitt, L. K. Oxenløwe, J. Wang, M. G. Thompson, and A. Laing, Generation and sampling of quantum states of light in a silicon chip, Nat. Phys. **15**, 925 (2019).
[22] H. J. McGuinness, M. G. Raymer, C. J. McKinstrie, and S. Radic, Quantum Frequency Translation of Single-Photon States in a Photonic Crystal Fiber, Phys. Rev. Lett. **105**, 093604 (2010).
[23] A. Farsi, Coherent manipulation of light in the classical and quantum regimes via four-wave mixing Bragg scattering, Ph.D. thesis, Cornell University, 2015.
[24] C. J. McKinstrie, S. Radic, and M. G. Raymer, Quantum noise properties of parametric amplifiers driven by two pump waves, Opt. Express **12**, 5037 (2004).
[25] C. J. McKinstrie, J. D. Harvey, S. Radic, and M. G. Raymer, Translation of quantum states by four-wave mixing in fibers, Opt. Express **13**, 9131 (2005).
[26] C. J. McKinstrie, M. Yu, M. G. Raymer, and S. Radic, Quantum noise properties of parametric processes, Opt. Express **13**, 4986 (2005).
[27] S. Clemmen, A. Farsi, S. Ramelow, and A. L. Gaeta, Ramsey Interference with Single Photons, Phys. Rev. Lett. **117**, 223601 (2016).
[28] M. Kues, C. Reimer, P. Roztocki, L. R. Cortés, S. Sciara, B. Wetzel, Y. Zhang, A. Cino, S. T. Chu, B. E. Little, D. J. Moss, L. Caspani, J. Azaña, and R. Morandotti, On-chip generation of high-dimensional entangled quantum states and their coherent control, Nature (London) **546**, 622 (2017).
[29] C. Reimer, S. Sciara, P. Roztocki, M. Islam, L. R. Cortés, Y. Zhang, B. Fischer, S. Loranger, R. Kashyap, A. Cino, S. T. Chu, B. E. Little, D. J. Moss, L. Caspani, W. J. Munro, J. Azaña, M. Kues, and R. Morandotti, High-dimensional one-way quantum processing implemented on d-level cluster states, Nat. Phys. **15**, 148 (2019).
[30] P. Imany, J. A. Jaramillo-Villegas, M. S. Alshaykh, J. M. Lukens, O. D. Odele, A. J. Moore, D. E. Leaird, M. Qi, and A. M. Weiner, High-dimensional optical quantum logic in large operational spaces, npj Quantum Inf. **5**, 59 (2019).
[31] J.-M. Mérolla, Y. Mazurenko, J.-P. Goedgebuer, and W. T. Rhodes, Single-Photon Interference in Sidebands of Phase-Modulated Light for Quantum Cryptography, Phys. Rev. Lett. **82**, 1656 (1999).
[32] L. Olislager, J. Cussey, A. T. Nguyen, P. Emplit, S. Massar, J.-M. Merolla, and K. P. Huy, Frequency-bin entangled photons, Phys. Rev. A **82**, 013804 (2010).
[33] L. Olislager, E. Woodhead, K. Phan Huy, J.-M. Merolla, P. Emplit, and S. Massar, Creating and manipulating entangled optical qubits in the frequency domain, Phys. Rev. A **89**, 052323 (2014).
[34] H.-H. Lu, J. M. Lukens, N. A. Peters, B. P. Williams, A. M. Weiner, and P. Lougovski, Quantum interference and correlation control of frequency-bin qubits, Optica **5**, 1455 (2018).
[35] P. Imany, O. D. Odele, M. S. Alshaykh, H.-H. Lu, D. E. Leaird, and A. M. Weiner, Frequency-domain Hong-Ou-Mandel interference with linear optics, Opt. Lett. **43**, 2760 (2018).
[36] H.-H. Lu, J. M. Lukens, N. A. Peters, O. D. Odele, D. E. Leaird, A. M. Weiner, and P. Lougovski, Electro-Optic Frequency Beam Splitters and Tritters for High-Fidelity Photonic Quantum Information Processing, Phys. Rev. Lett. **120**, 030502 (2018).
[37] B. Galmès, K. Phan-Huy, L. Furfaro, Y. K. Chembo, and J.-M. Merolla, Nine-frequency-path quantum interferometry over 60 km of optical fiber, Phys. Rev. A **99**, 033805 (2019).
[38] T. Kobayashi, R. Ikuta, S. Yasui, S. Miki, T. Yamashita, H. Terai, T. Yamamoto, M. Koashi, and N. Imoto, Frequency-domain Hong–Ou–Mandel interference, Nat. Photonics **10**, 441 (2016).
[39] See Supplemental Material at http://link.aps.org/supplemental/10.1103/PhysRevLett.124.143601 for explicit theoretical calculations, details of experimental setup, single-photon source performance, system loss characterization, and a qualitative comparison of our scheme with alternative EOM-based schemes.

[40] Z. Vernon, M. Menotti, C. C. Tison, J. A. Steidle, M. L. Fanto, P. M. Thomas, S. F. Preble, A. M. Smith, P. M. Alsing, M. Liscidini, and J. E. Sipe, Truly unentangled photon pairs without spectral filtering, Opt. Lett. **42**, 3638 (2017).

[41] T. Legero, T. Wilk, M. Hennrich, G. Rempe, and A. Kuhn, Quantum Beat of Two Single Photons, Phys. Rev. Lett. **93**, 070503 (2004).

[42] T. Legero, T. Wilk, A. Kuhn, and G. Rempe, Time-resolved two-photon quantum interference, Appl. Phys. B **77**, 797 (2003).

[43] A. Christ and C. Silberhorn, Limits on the deterministic creation of pure single-photon states using parametric down-conversion, Phys. Rev. A **85**, 023829 (2012).

[44] D. Bonneau, G. J. Mendoza, J. L. O'Brien, and M. G. Thompson, Effect of loss on multiplexed single-photon sources, New J. Phys. **17**, 043057 (2015).

[45] P. Roztocki, M. Kues, C. Reimer, B. Wetzel, B. E. Little, S. T. Chu, D. J. Moss, and R. Morandotti, Pulsed quantum frequency combs from an actively mode-locked intra-cavity generation scheme, in *2017 Conference on Lasers and Electro-Optics, OSA Technical Digest (online)* (Optical Society of America, 2017), paper FW4E.4.

[46] I. Agha, M. Davanço, B. Thurston, and K. Srinivasan, Low-noise chip-based frequency conversion by four-wave-mixing Bragg scattering in SiN_x waveguides, Opt. Lett. **37**, 2997 (2012).

[47] Q. Li, M. Davanço, and K. Srinivasan, Efficient and low-noise single-photon-level frequency conversion interfaces using silicon nanophotonics, Nat. Photonics **10**, 406 (2016).

[48] K. Li, H. Sun, and A. C. Foster, Four-wave mixing Bragg scattering in hydrogenated amorphous silicon waveguides, Opt. Lett. **42**, 1488 (2017).

[49] B. A. Bell, C. Xiong, D. Marpaung, C. J. McKinstrie, and B. J. Eggleton, Uni-directional wavelength conversion in silicon using four-wave mixing driven by cross-polarized pumps, Opt. Lett. **42**, 1668 (2017).